TECHNICAL PAPER

Effect of multi-infill patterns on tensile behavior of FDM printed parts

Harshit K. Dave[1] · Brijesh H. Patel[1] · Shilpesh R. Rajpurohit[1] · Ashish R. Prajapati[1] · Dumitru Nedelcu[2]

Abstract

Fused Deposition Modeling (FDM) is an extrusion-based additive manufacturing technique which growing rapidly due to its ability to fabricate complex parts directly from CAD models. In conjunction with its growing applications, the mechanical behavior of the FDM printed part needs thorough investigation for effective application as an end use functional part in various industries such as aerospace, automobile, mold and die, biomedical. Functional applications of FDM printed parts are affected due to their lower mechanical properties compared to injection molded parts. The assessment of the mechanical behavior of the FDM printed part is proved as challenging task due to the wide variety of the process parameters. In the present work, an attempt has been made to experimentally investigate the tensile behavior of FDM printed parts having multi-Infill patterns and different stacking of layer arrangements for different Infill density and raster orientations. Combined patterned parts are printed from two thermoplastic materials, viz. PLA and ABS having six different stacking sequences at three different levels of Infill density (i.e., 30%, 60% and 90%) and two different raster arrangements (i.e., 0° and 45°) and those are mechanically tested to obtain tensile properties. Further, the fractographic analysis was carried out to study various aspects of tensile failure modes for FDM printed multi-infill pattern samples. Combining two different infill patterns and layer stacking sequence improves tensile strength for 45° raster orientation samples and decreases tensile strength for 0° raster orientation samples when compared to a single pattern throughout. For 0° raster orientation, stacking sequence with all the layers are deposited parallel to loading direction offers more strength than multi-infill pattern samples. Whereas for 45° raster orientation, stacking sequence with all the layers parallel to loading direction offers lower strength than multi-infill pattern samples.

Keywords Fused deposition modeling · Multi-infill patterns · Stacking sequence · Raster orientation · Infill density · Tensile strength

Technical Editor: João Marciano Laredo dos Reis.

✉ Harshit K. Dave
  harshitkumar@yahoo.com

  Brijesh H. Patel
  brijeshnkd@gmail.com

  Shilpesh R. Rajpurohit
  shilpesh18@gmail.com

  Ashish R. Prajapati
  iamarp5155@gmail.com

  Dumitru Nedelcu
  nedelcu1967@yahoo.com

1 Department of Mechanical Engineering, Sardar Vallabhbhai National Institute of Technology, Surat, Gujarat 395 007, India

2 Department of Machine Manufacturing Technology, "Gheorghe Asachi" Technical University of Iasi, Str Prof Dr Doc Dumitru Mangeron No. 59A, 700050 Iasi, Romania

1 Introduction

Fused Deposition Modeling (FDM) is one of the popular additive manufacturing techniques by which part is built layer-by-layer directly from CAD model. Initially, based on conceptual design, a geometric model is created and then converted to standard tessellation language (STL) file format, which approximates the surfaces of the model as a triangle. Apart from STL file format, models can also be converted into AMF, OBJ, 3MF and DAE via CAD software. In addition, the 3D scanning systems are also used to make 3D model by reverse engineering process [1]. Now the model is sliced in very thin layers by using slicing software and G-code file is generated for the model. At last generated file is loaded into the FDM software, which governs the process and part is built layer-by-layer.

During FDM printing, the filament from the spool is fed into the extrusion head and is heated to a semi-liquid state. Now, this semi-liquid state material is extruded and deposited on the heated bed in a layer by layer fashion to fabricate the part. Once a layer is deposited, the bed is lowered as per the defined layer thickness for further deposition of material. The entire part is fabricated by depositing material in successive layers. Once the part is developed and solidifies, it is removed from the bed for post-treatments if needed [2].

FDM is a widely accepted additive manufacturing technique because it shortens the time of product development and it is easy to fabricate complex parts due to layer-wise material deposition directly from CAD model without any specific requirement of tooling. The mechanical behavior of FDM printed parts depends on the various process parameters and can be affected by the selection of process parameters [3, 4]. Mechanical strength and accuracy of parts can be enhanced by following build rules while printing [5]. Optimization of process parameters improves mechanical performance and parts can be directly used in functional applications [6], and the microstructure of FDM material has a pronounced effect on mechanical performance [7]. FDM printed samples exhibit lower mechanical strength than injection molded samples [5–9].

Durgun and Ertan [10] investigated the effect of raster angle and build orientation on strength, surface roughness and production cost of FDM printed ABS samples. Test results confirmed that 0° raster angle and horizontal build direction show optimal mechanical performance and surface roughness with optimum production cost and time. Li et al. [11] confirmed that layer height has a major impact on bonding strength followed by deposition velocity. On the other hand, infill rate has a negligible effect. Casavola et al. [12] used classical laminate theory to characterize the mechanical behavior of FDM parts. Both young's modulus and UTS showed a reduction with an increase in raster angle from 0° to 90° and 45° samples exhibit an intermediate mechanical behavior. Chacon et al. [13] carried out a tensile test and flexural test to investigate the effect of build orientation, feed rate and layer thickness and observed optimal mechanical performance for lower layer thickness and high feed rate. On-edge orientation offered the highest strength followed by flat orientation and least strength for upright orientation. Rajpurohit and Dave [14] confirmed that 0° raster angle and lower layer height offer higher Tensile strength. Tensile strength increased with an increase in raster width up to a certain extent, then it decreased. Dave et al. [15] observed higher tensile strength for specimens with rectilinear and concentric infill patterns built-in flat and on long edge orientation as compared to on short edge orientation. They also reported that specimen with Hilbert curve infill pattern showed better results for short edge orientation as compared to long edge orientation. Rodriguez et al. [16]

observed a reduction in strength of FDM samples due to the presence of voids and loss of molecular orientation during extrusion when compared to the strength of ABS monofilament. Lederle et al. [17] carried out material extrusion under the inert gas atmosphere and observed enhanced mechanical performance for both materials (ABS and nylon copolymer) when compared to samples printed in the open air. Wu et al. [18] observed 108% higher tensile strength, 114% higher compressive strength and 115% higher bending strength for polyether-ether-ketone (PEEK) samples than ABS samples. Ziemian et al. [19] observed better fatigue life under tension-tension fatigue test for 0° and +45°/−45° raster orientation when compared to diagonal (45°) and transverse (90°) raster orientations. Zaldivar et al. [20] studied the effect of build orientation on mechanical and thermal properties of FDM printed ULTEM samples and observed variation in the coefficient of thermal expansion for different orientations. Alvarez et al. [21] observed higher printing time and lesser tensile strength for infill of 50–98% when compared to 100% infill for hexagonal infill pattern. Shih et al. [22] observed an improvement of interlayer bonding strength in cold plasma treated PLA samples when compared to untreated samples. They also observed that treatment time adversely affecting the bonding strength. Lee and Liu [23] studied the effect of forced air cooling on FDM printed PLA samples and observed improved dimensional quality and decreased mechanical strength at higher airflow velocity (5 m/s). Ishak et al. [24] carried out material deposition in different planes in a single part for different build orientations. They observed improvement in ultimate tensile strength, modulus of elasticity and yield strength for the upright printed specimens. Different approaches have also been used to investigate the mechanical properties of FDM part, such as FE simulations [25–28], addition fiber reinforcement in FDM parts [29–32], ultrasonic strengthening of printed part [33], and Damage/deformation study [34]. Apart from that, researchers have investigated the effect of chemical treatment on FDM printed part on the mechanical properties. Kozior et al. [35] successfully combined FDM printing and electrospinning in order to prepare mechanically stable filters with a Nano fibrous surface. Effect of adhesion of FDM printed polymers on textile fabrics has also been investigated [36]. A study showed that applying the chemical treatment on the FDM printed parts resulted in good surface texturing. However, due to the chemical treatment, tensile strength is reduced [37].

The majority of the work has been reported on the effect of various process parameters, viz. raster angle, build orientation, infill strategies, layer thickness, raster width, air gap, print temperature, bed temperature, etc. To date, the majority of the work has been reported on the tensile properties of the FDM part with a single infill pattern throughout. To the best of the author's knowledge, no work is reported on the effect

of multi-infill patterns and layer stacking sequences on the tensile properties of FDM parts. There is a requirement of a study on the effect of single and multi-infill patterns on tensile properties of FDM printed part for a better understanding of infill strategy. Hence, in this study, an experimental investigation was carried out to understand the effect of a multi-infill pattern at different infill density raster orientation and stacking sequences on the tensile properties of FDM printed ABS and PLA parts. To fabricate the specimen, customized G-code files were prepared to print multi-infill pattern specimens and the uniaxial tensile test was carried out to investigate mechanical response in terms of tensile strength. Further, the microscopic examination of fractured surfaces was carried out to understand the effect of a multi-infill pattern on the failure mode of printed specimens.

2 Materials and methods

2.1 Experiment design

The objective of the present work is to study the effect of multi-infill patterns with different raster orientation and different infill density under different stacking sequence of layers on tensile strength of FDM printed parts. Tensile testing specimens were printed with rectilinear and grid as infill patterns at two different raster orientations, viz. 0° and 45° with

the longitudinal axis of the part (i.e., x-axis of the machine). Infill density has been varied at three levels i.e., 30%, 60% and 90%. Figure 1 illustrates the variation of slicing parameters. Layers of the specimens were arranged in six different stacking sequences, viz. S1, S2, S3, S4, S5 and S6 as shown in Fig. 2 and details for different stacking sequences, are given in Table 1. The process parameter levels and their values are shown Table 2. In the present investigation, samples were printed from two thermoplastic materials, viz. Polylactic Acid (PLA) and Acrylonitrile Butadiene Styrene (ABS). PLA is bio-based and biodegradable polymer whose properties are comparable to the other plastics in the industry. ABS is petroleum-based, non-biodegradable plastic which is widely used in electronic industry, automobile industry, pipe fittings and toy industry. Table 3 shows the properties of PLA and ABS filaments. In this study, full factorial experimental design was considered and a total of 36 specimens with a different combination of process parameters have been selected for printing for each material. All the specimens were printed thrice to ensure the repeatability of experiments. Hence, a total of 108 nos. of PLA specimens and 108 nos. of ABS specimens were printed and tested.

Tensile test specimens were fabricated as per the ASTM D638 standard having a thickness of 3.2 mm. Figure 3 illustrates a schematic of the test specimen. Layer height for the printing was chosen as 0.1 mm. Hence, one specimen contains 32 layers, out of which top and bottom layers are

Fig. 1 Variation of slicing parameters
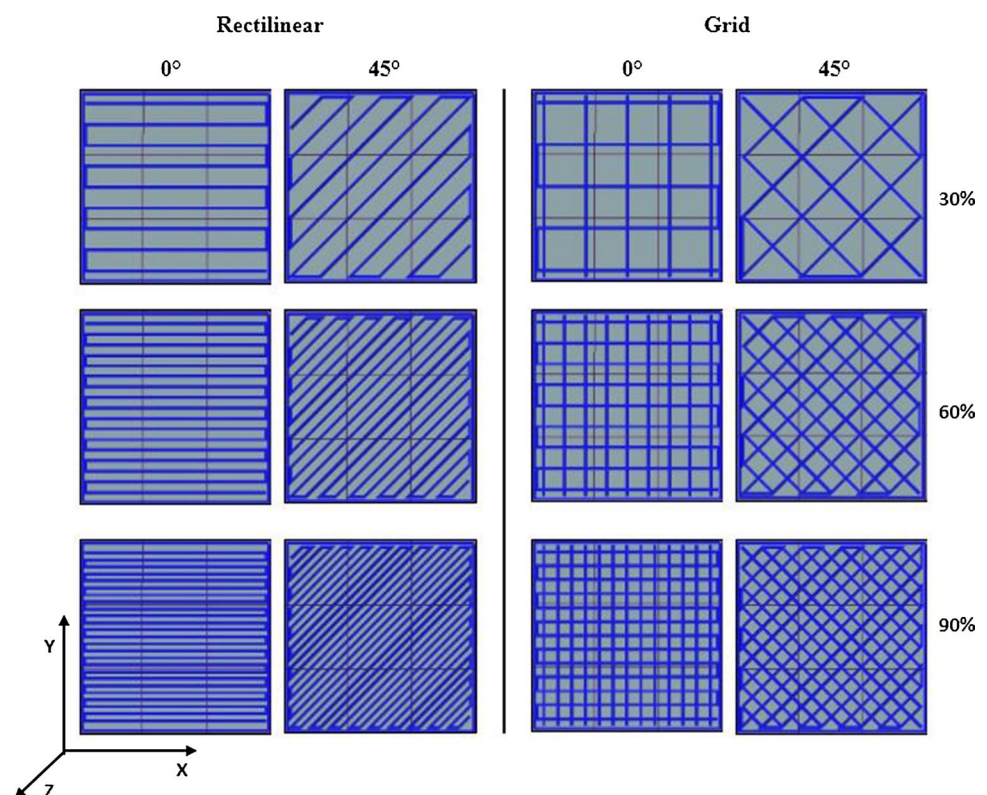
Fig. 2 Different stacking sequences of layer arrangement
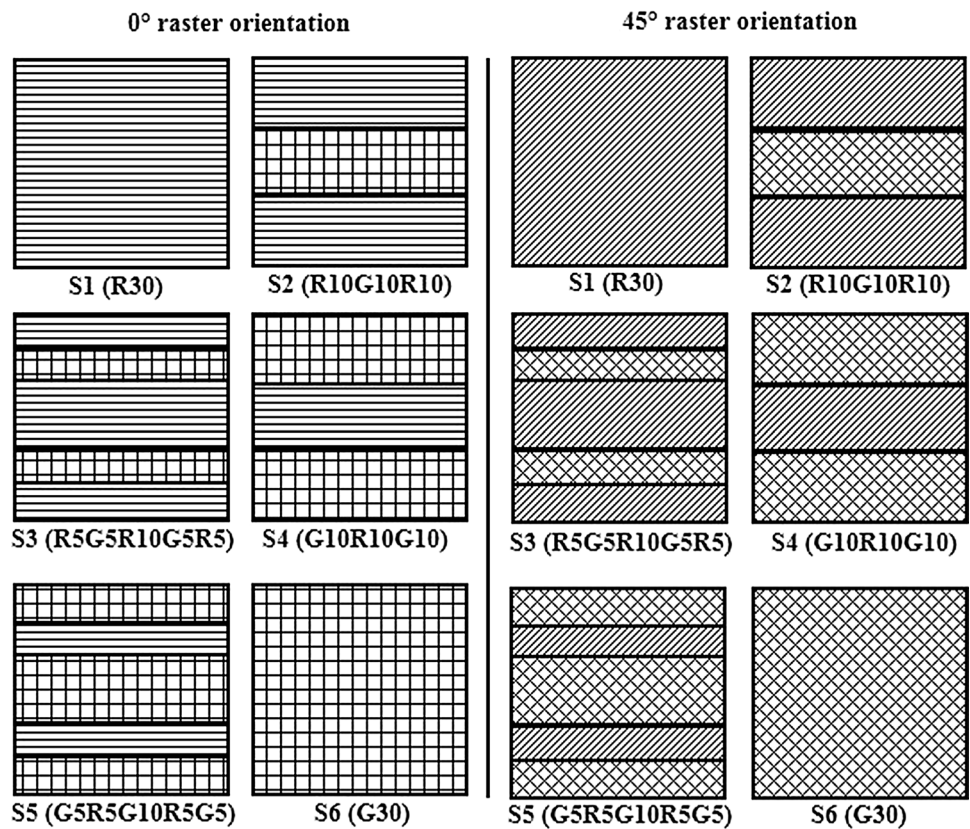
Table 1 Description of layer arrangement for different stacking sequences

Stacking sequence	Designation	Description
S1	R30	All 30 layers are of a rectilinear type
S2	R10G10R10	The first 10 layers are of rectilinear type, then 10 layers at the middle are of grid type and 10 layers at the top are of rectilinear type
S3	R5G5R10G5R5	The First 5 layers are of rectilinear type, next 5 layers are of grid type, 10 layers at the middle are of rectilinear type, next five layers are of grid type and 5 layers at the top are of rectilinear type
S4	G10R10G10	The first 10 layers are of grid type, then 10 layers at the middle are of rectilinear type and again 10 layers at the top are of grid type
S5	G5R5G10R5G5	The first 5 layers are of grid type, then next 5 layers are of rectilinear type, 10 layers at the middle are of grid type then again 5 layers are of rectilinear type and 5 layers at the top are of grid type
S6	G30	All 30 layers are of grid type

**Table 2** Process parameters and their values

Raster orientation	Infill density (%)	Infill stacking sequence
0°	30	S1 to S6
	60	S1 to S6
	90	S1 to S6
45°	30	S1 to S6
	60	S1 to S6
	90	S1 to S6

Table 3 PLA and ABS filament properties (manufacturer's datasheet)

Property	PLA	ABS
Print temperature (°C)	205–225	220–260
Bed temperature (°C)	60–80	90–110
Tensile strength (MPa)	65	43
Elongation at break (%)	12	22
Flexural strength (MPa)	75	66
Impact strength (kJ/m^2)	8.5	19

Fig. 3 Schematic of tensile test specimen as per ASTM D638 (All the dimensions are in mm)
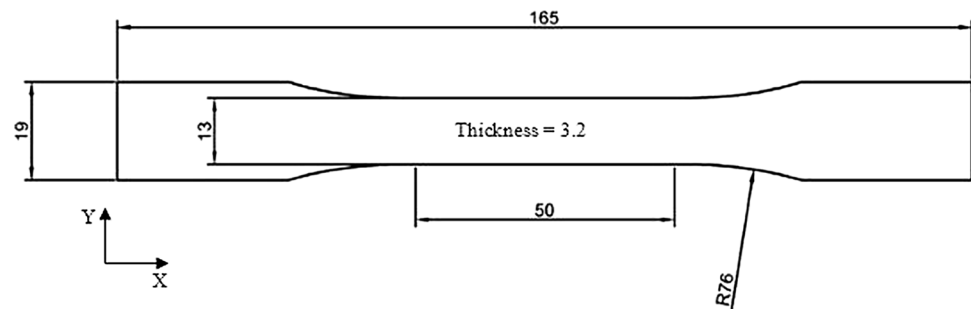
Table 4 Constant parameters during printing

Parameter	PLA	ABS
Layer height (mm)	0.1	0.1
Raster width (mm)	0.5	0.5
Bed temperature (°C)	70	90
Nozzle temperature (°C)	210	250
Printing speed (mm/s)	40	40
No. of perimeters	1	1

printed as solid layers. So infill pattern, infill density and stacking sequence are varied for the remaining 30 layers.

2.2 Specimen fabrication

In the present study, test specimens were printed on using open source desktop type high precision OMEGA dual extruder FDM 3D printer with a build volume of $500 \times 500 \times 500$ mm. All the samples were printed in flat orientation i.e., all the layers are parallel to the XY plane and the thickness of the specimen can be seen in Z-direction and the longitudinal axis of the specimen is similar to the X-axis of the machine. A filament with 1.75 mm diameter was extruded through a nozzle of 0.4 mm diameter and customized tool path files were created to print multi-infill pattern samples. Fixed parameters and their values are given in Table 4.

2.3 Tensile testing

Uniaxial tension test was performed to evaluate tensile strength using horizontal type electronic tensometer, PC-2000 (Make: Kudale Instruments Pvt. Ltd., India) with a 20 kN load capacity. Tensile tests were performed as per the ASTM D638 standard with a deformation speed of 5 mm/min until specimen failure occurs at room temperature. Stress–strain, load, elongation data were monitored and recorded by the built-in software of the electronic tensometer. Figure 4 shows the test specimen held in cross–wedge gripper for tensile testing.

3 Results and discussion

In the present work, an investigation was carried out to study the tensile behavior of multi-infill patterned FDM printed parts for different stacking sequences of layers. All the experiments were performed as per experimental design as discussed earlier and tested. The result obtained through tensile testing of FDM specimens with a multi-infill pattern is discussed in this section.

Figure 5 depicted the effect of the stacking sequence and multi-infill pattern on the tensile strength of the FDM part at different raster orientation and percentage infill. At 0° raster orientation, the highest strength is observed for a specimen having stacking sequence S1 and the lowest strength is observed for stacking sequence S6 for all considered infill density. In the case of 45° raster orientation, stacking sequences S1 and S6 show similar strength, whereas stacking sequences S3 and S5 show similar strength i.e., for PLA samples, 9.33 MPa for S1 and 9.23 MPa for S6 at 30% infill density; 22.1 MPa for S1 and 24.5 MPa for S6 at 90% infill density. Whereas for ABS samples, 7.7 MPa for S1 and 8.6 MPa for S6 at 30% infill density; 14.4 MPa for S1 and 15.1 MPa for S6 at 60% infill density.

Figures 6, 7, 8, 9, 10 and 11 show the fractured surface of specimens having stacking sequence S1 to S6. Higher tensile strength is obtained at S1 stacking sequence with 0° raster orientation. In contrast, lower tensile strength is obtained at S6 stacking sequence. The difference in tensile strength for multi-infill pattern samples can be explained by failure modes associated with them. Parts having stacking sequence S1 have trans-raster failure, whereas stacking sequence S6 has inter raster failure i.e., failure at raster meeting junction. S1 stacking sequence has all the layers deposited parallel to loading direction during the tensile test. Due to the parallel arrangement of the beads and loading direction, the individual bead is capable of bearing more load and failure occurred due to the breakage of each bead. It is observed that grid layers are weaker than rectilinear layers due to the improper fusion at the grid junction, where two raster perpendicular to each other bond with each other. The strength of bond depends on the fusion of material at the raster interface and weaker bond formed at the raster interface due to

Fig. 4 Mikrotech PC-2000 tensile testing setup
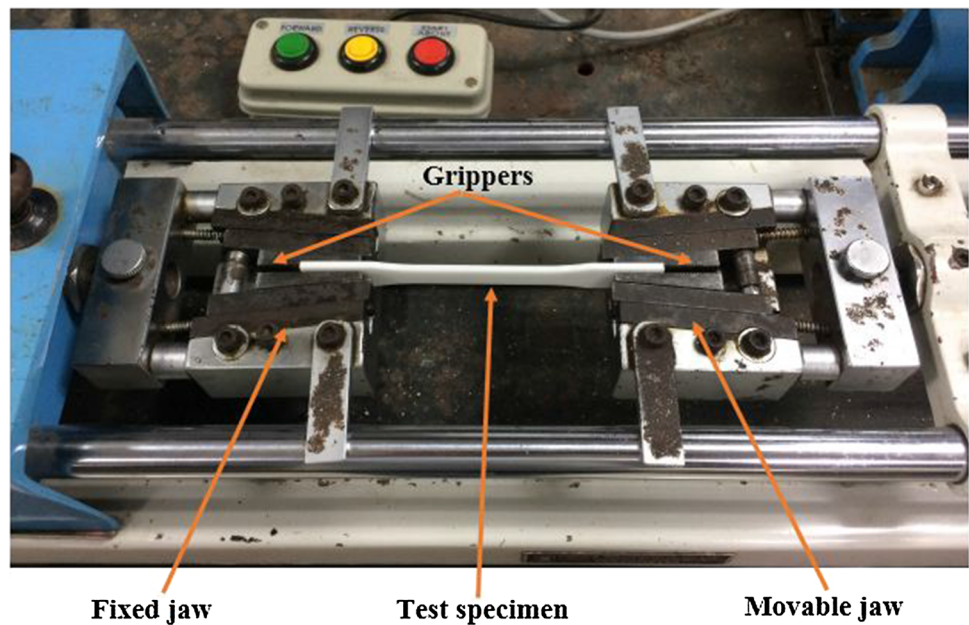
the incomplete fusion bond. Moreover, these junction points also act as stress concentration points and failure occurred due to breakage of bonding at the junction points. Parts with multi-infill patterns (i.e., S2, S3, S4 and S5) experiences a mixed failure mechanism (both trans-raster and inter raster failure).

It is observed that samples were having stacking sequence S1 and S6 offer nearly similar tensile strength at 45° raster orientation because of less material availability to resist applied load (45°-S1) and weak inter raster bonding (45°-S6). Figure 12 shows the fractured surface of the specimen having stacking sequence S1 at 45° raster orientation. Due to the absence of fusion between adjacent rasters, the applied load is taken by the outer shell and a single stacked column of rasters and failure occurs due to breakage of individual rasters in a single stacked column. On the other hand, samples having stacking sequence S6 at 45° raster orientation, failure occurs at the region where two rasters fuse and make a bond. These raster meeting junction points act as stress concentration points and because of weak bonding between rasters, failure takes place. In the S6 stacking sequence, more material is available to bear applied load but incomplete fusion at the junction is responsible for lower strength. Figure 13 shows the fractured surface of the specimen having stacking sequence S6 at 45° raster orientation.

The incorporation of grid layers decreases the strength in the case of 0° raster orientation samples as moving from S1 to S6. S1 offers more strength than that of the strength offered by multi-infill pattern samples. Whereas, in the case of 45° raster orientation samples, S1 offers lower strength than that of the strength offered by multi-infill pattern samples. The fractured surface of the multi-infill pattern part

with 45° raster orientation is shown in Fig. 14. It is visible that failure occurs due to the breakage of rasters of rectilinear pattern and breakage at the bonding region of the grid pattern. For multi-infill pattern samples, grid layers provide support to rectilinear layers and the number of stacked columns of rasters becomes available to bear applied load instead of a single stacked column in the case of S1.

As moving from stacking sequence S1 to S6, the number of grid layers increases from 0 (for S1) to 30 (for S6). Out of total 30 layers, stacking sequences S2 and S3 contain 10 layers of the grid pattern and 20 layers of a rectilinear pattern, but they differ in their arrangement i.e., for stacking sequence S2 all grid layers are located at mid-region of part, whereas for stacking sequence S3 grid layers are split into two groups of five-layer each and arranged at the upper side and lower side of 10 rectilinear layers as shown in Fig. 15. Splitting of layers does not offer any considerable effect on tensile strength i.e., for 0°-PLA samples, 18.5 MPa for S2 and 18.9 MPa for S3 at 30% infill density; 26.2 MPa for S2 and 27 MPa for S3 at 60% infill density; 36.3 MPa for S2 and 35.1 MPa for S3 at 90% infill density. Similarly, stacking sequences S4 and S5 contain 10 rectilinear layers. For S4 all rectilinear layers are arranged at mid-region, whereas for S5 they are split into two groups of five layers each and located at the upper and lower side of ten grid layers. Stacking sequences S4 and S5 show similar strength i.e., for 0°-ABS samples, 13.1 MPa for S4 and 13.2 MPa for S5 at 30% infill density; 17.3 MPa for S4 and 20.1 MPa for S5 at 60% infill density; 28.5 MPa for S4 and 27.6 MPa for S5 at 90% infill density. Similar observations have been made for 45°-PLA and ABS samples that can be seen in Fig. 5. For all considered print settings, PLA samples show higher tensile
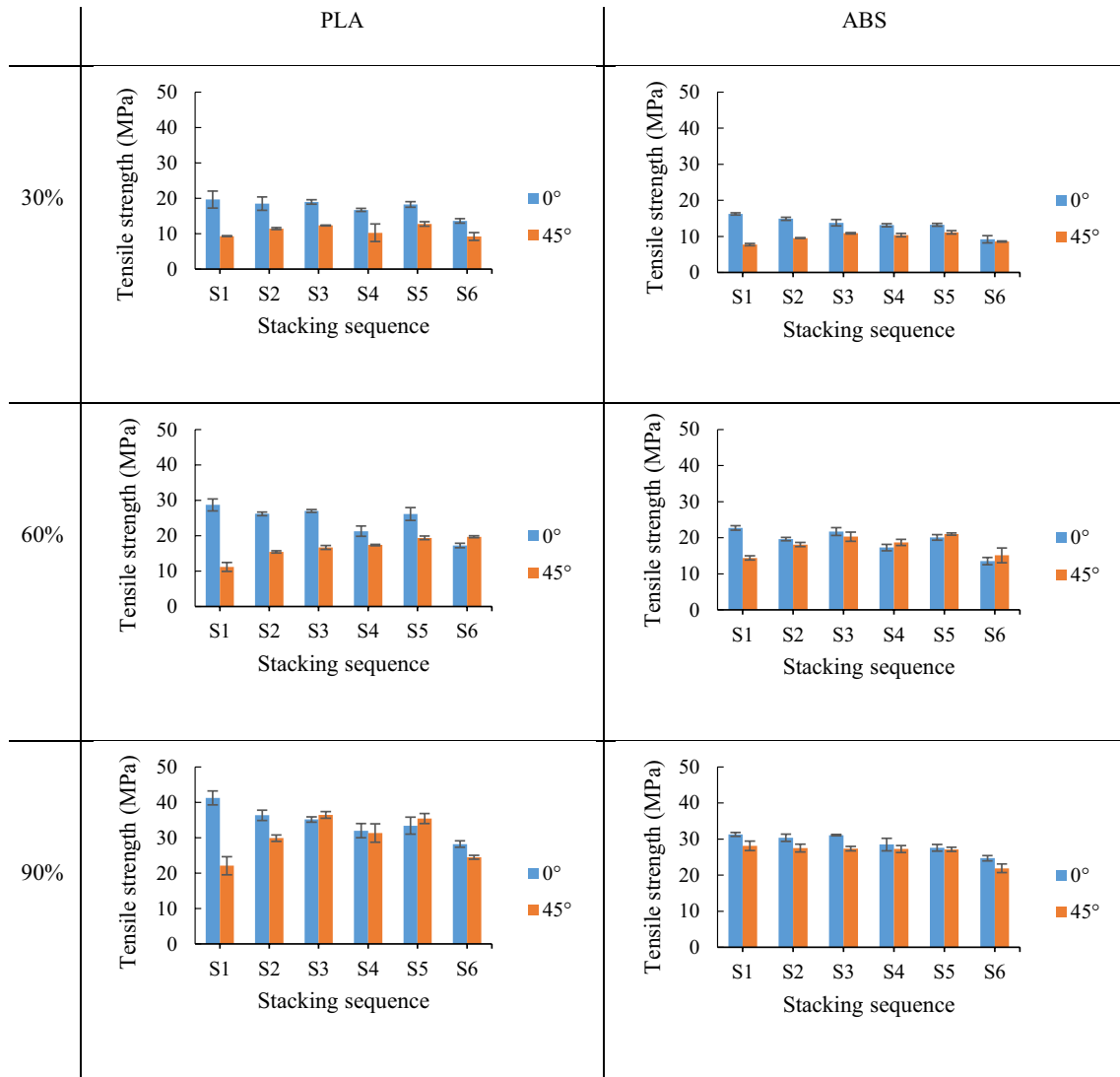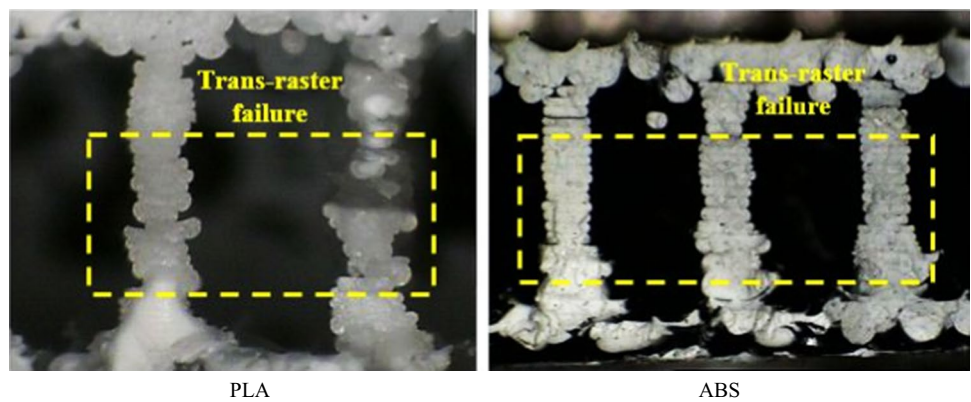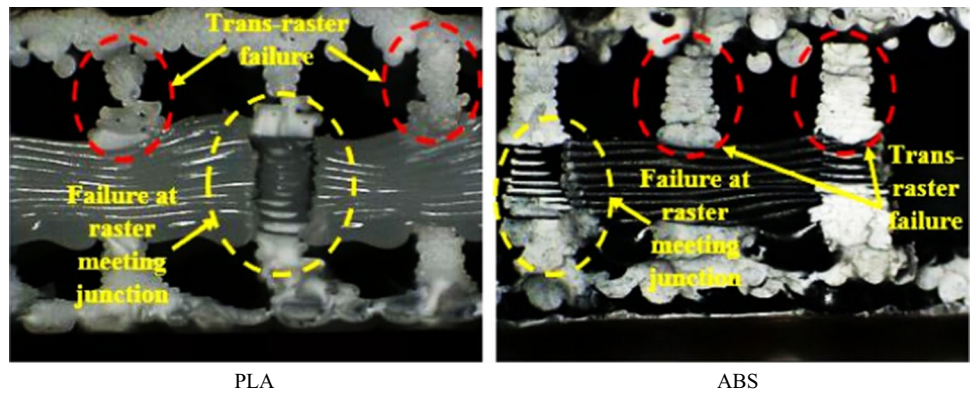
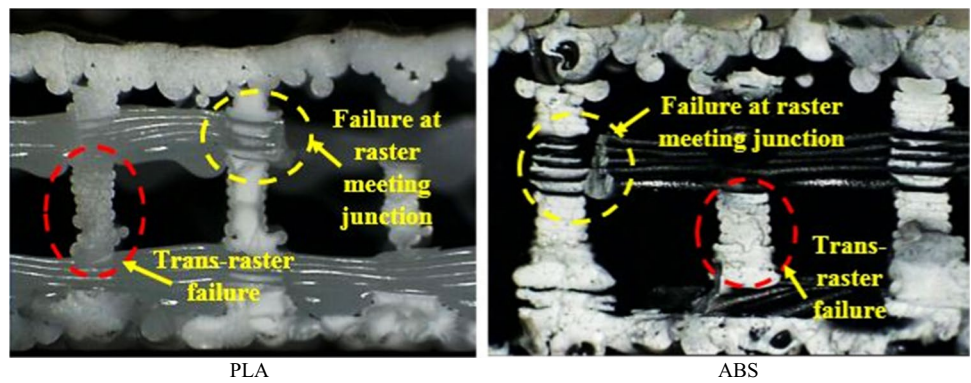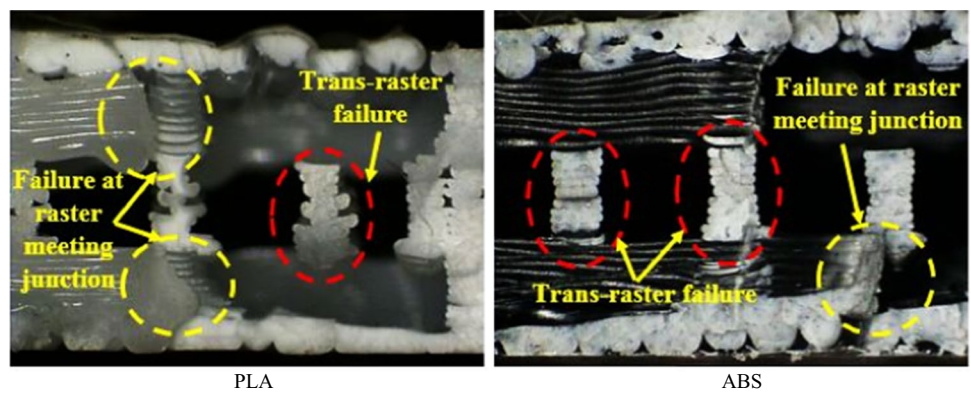**Fig. 5** Effect of stacking sequence and multi-infill patterns on tensile strength

Fig. 6 Fractured surface of specimen having stacking sequence S1 at 30% infill

Fig. 7 Fractured surface of specimen having stacking sequence S2 at 30% infill
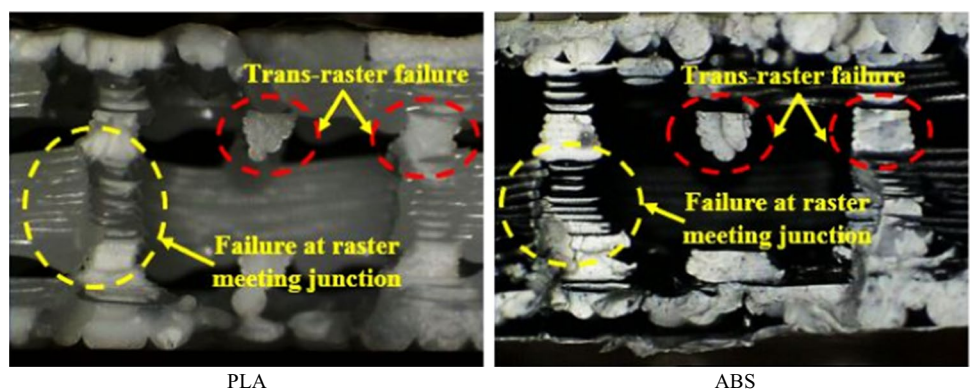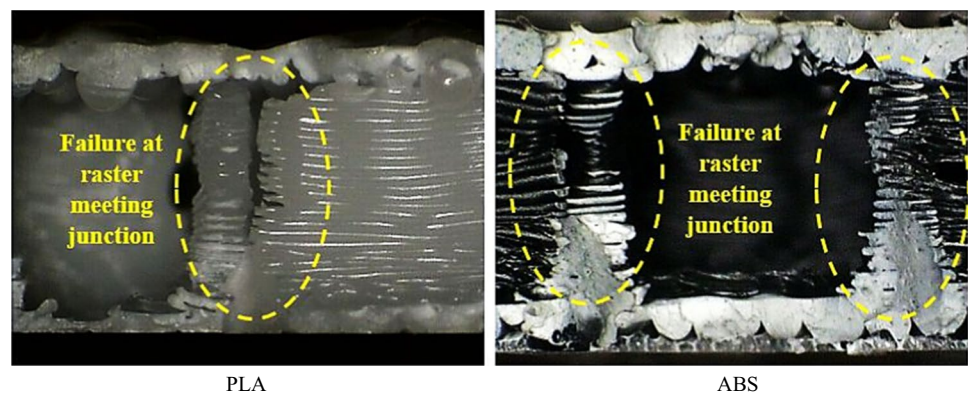

PLA

ABS

Fig. 8 Fractured surface of specimen having stacking sequence S3 at 30% infill

PLA

ABS

Fig. 9 Fractured surface of specimen having stacking sequence S4 at 30% infill

PLA

ABS

Fig. 10 Fractured surface of specimen having stacking sequence S5 at 30% infill

PLA

ABS

Fig. 11 Fractured surface of specimen having stacking sequence S6 at 30% infill

PLA   ABS

Fig. 12 Fracture surface of specimen having stacking sequence S1 at 45° raster orientation (**a**) PLA and (**b**) ABS


(a)

(b)
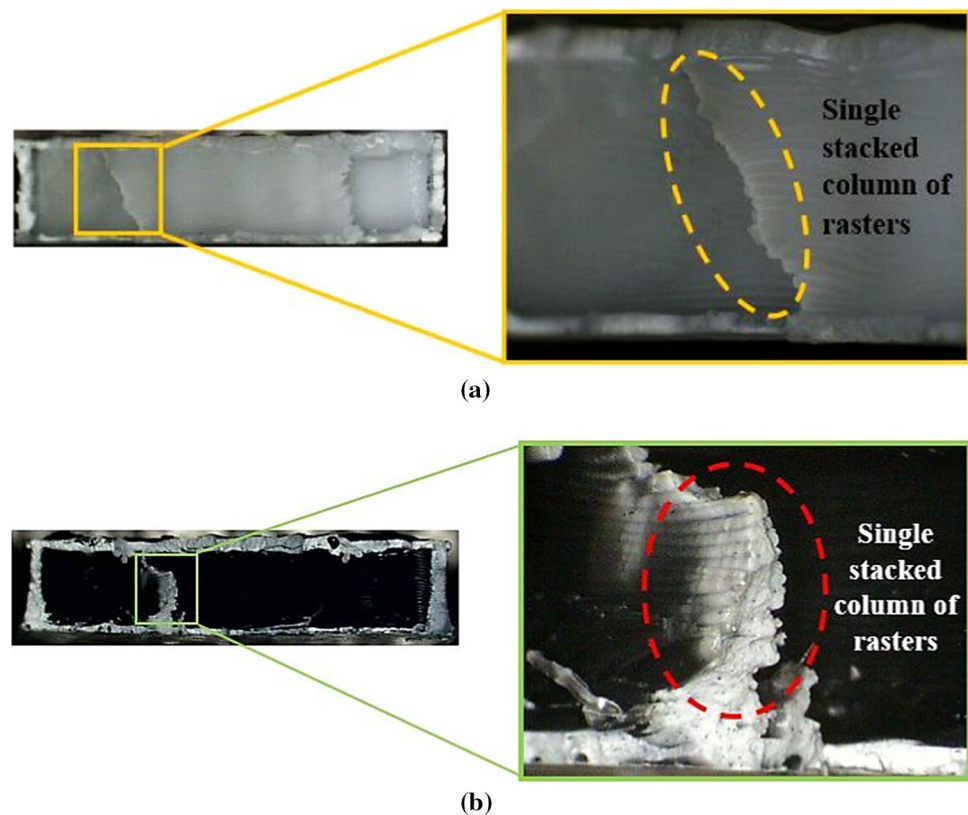
strength than that of ABS samples. The mechanical properties of FDM printed parts highly depend on the various process parameters apart from filament material properties and can be affected by the selection of process parameters. Hence, the highest strength offered by FDM printed samples for both the materials is less than the strength of filament material.

Figure 16 shows the effect of infill density on tensile strength for different stacking sequences and different raster orientation. It is observed that tensile strength increases with an increase in infill density i.e., highest tensile strength is observed for samples having 90% infill density. In comparison, 30% infill density resulted in lower tensile strength.

Specimens with 60% infill density displayed intermediate strength for all stacking sequences and raster orientations.

It is observed that tensile strength increases with an increase in infill density for all the raster orientations and all the stacking sequences. The increase in strength with increment in infill density is observed due to the availability of more load resisting material and the presence of intra-raster bonding at higher infill density. It is observed that a higher bonding area takes place between rasters of layers closer to the bed. The bed is heated at elevated temperature and because of continuous heat supply to the layers, intra-raster necking takes place due to that bottom layers become near to solid. Figure 17 shows the fractured surface of specimens
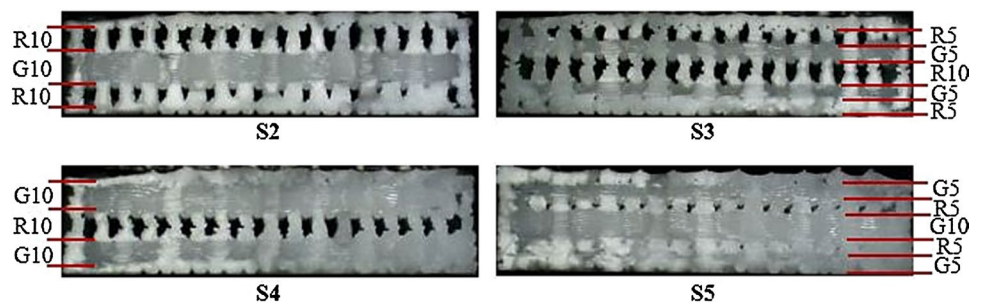
Fig. 13 Fracture surface of specimen having stacking sequence S6 at 45° raster orientation
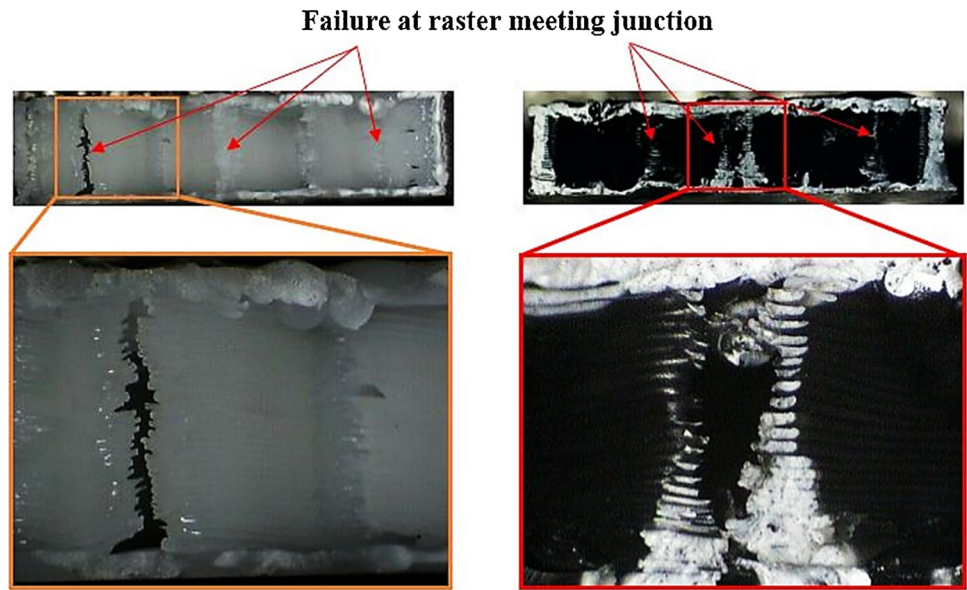
Fig. 14 Fracture surface of multi-infill pattern sample at 45° raster orientation
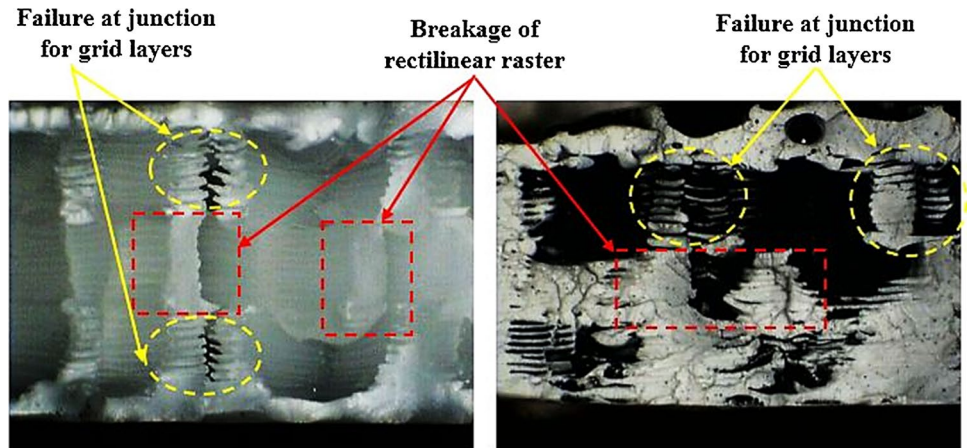
Fig. 15 Cross-sectional view of multi-infill pattern samples

having different infill density for both materials. There is an absence of intra-raster bonding at lower infill density because of the larger gap between deposited rasters. Due to the effect of bed heating, solid layers are observed near the bed in higher infill density specimens. The effect of bed heating is also observed in multi-infill pattern parts that can be seen in Fig. 18. Inter-raster fusion is restricted to some

layers, after that no fusion occurs because of solid layers near the bed act as resistance to heat flow.

Figure 19 shows the effect of raster orientation on tensile strength for different stacking sequences at different infill density. It can be seen that for stacking sequence S1, samples with 0° raster orientation show significantly higher strength than 45° raster orientation for all infill density.
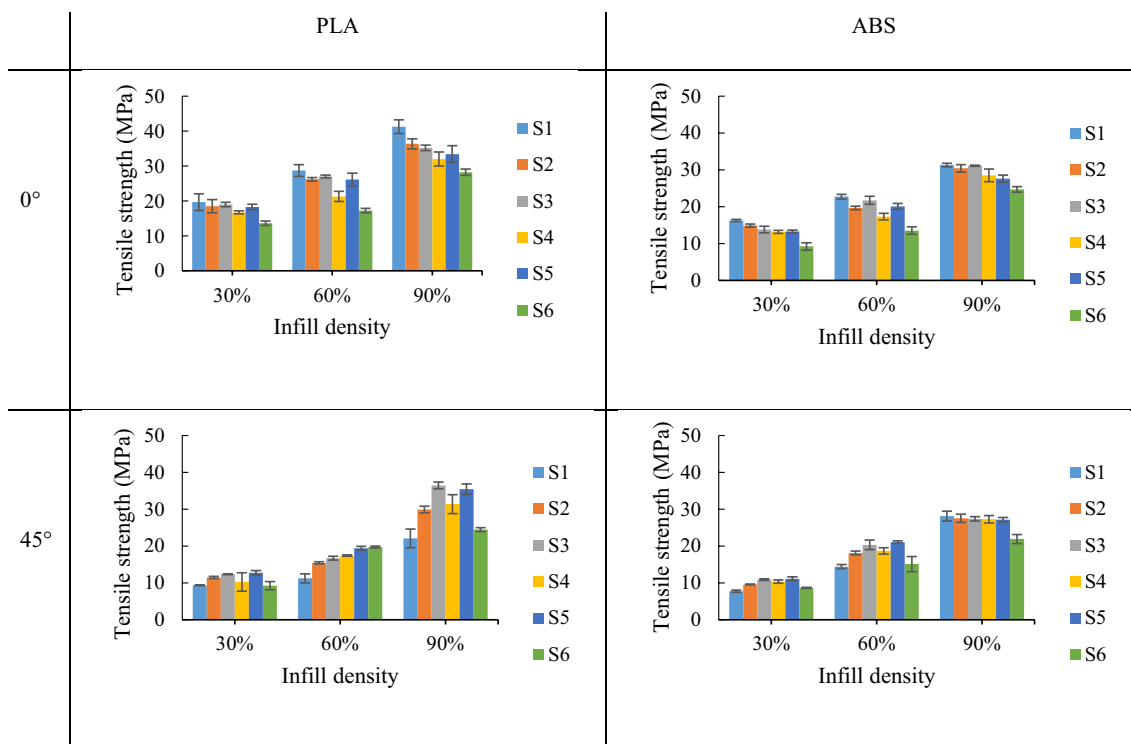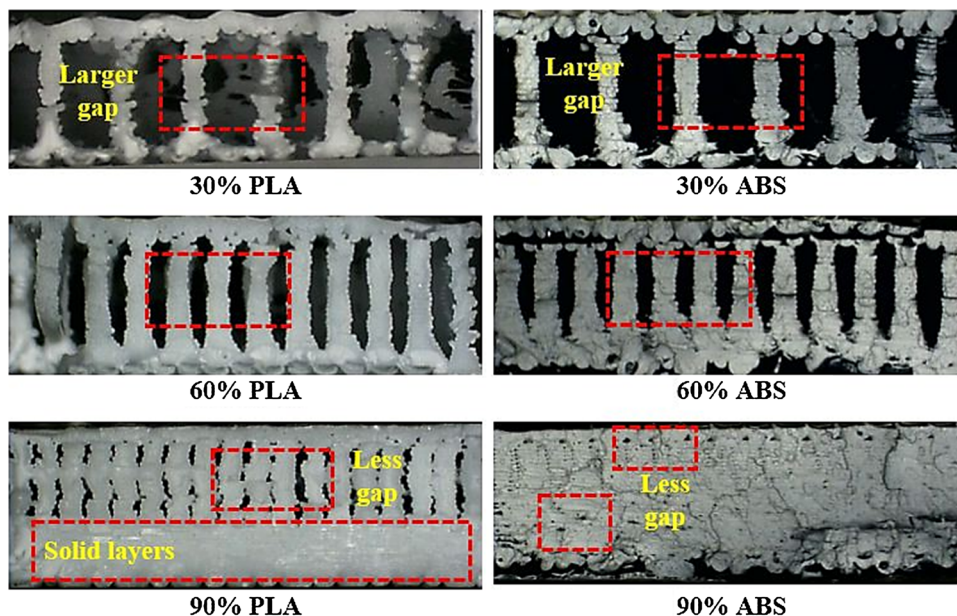
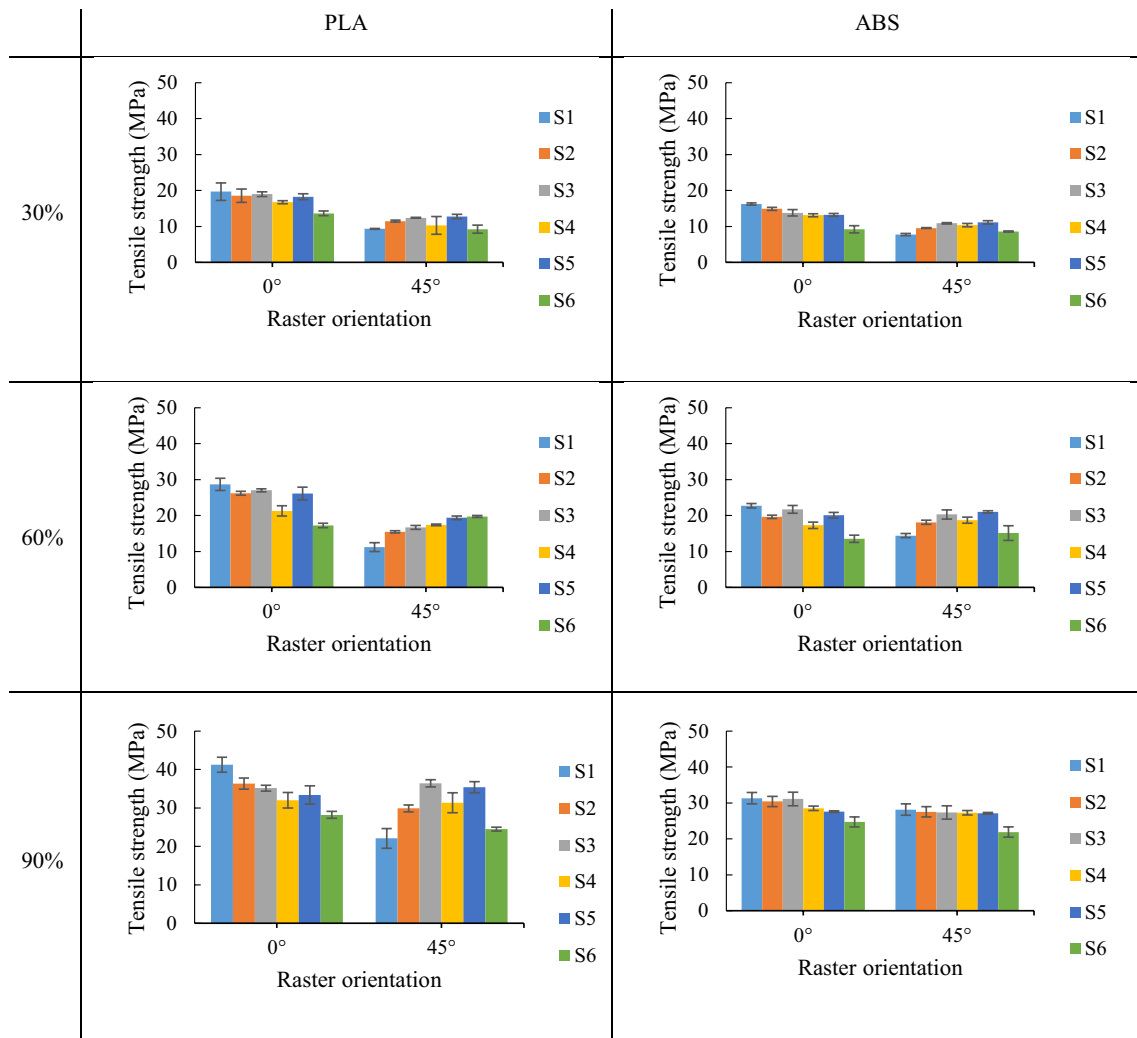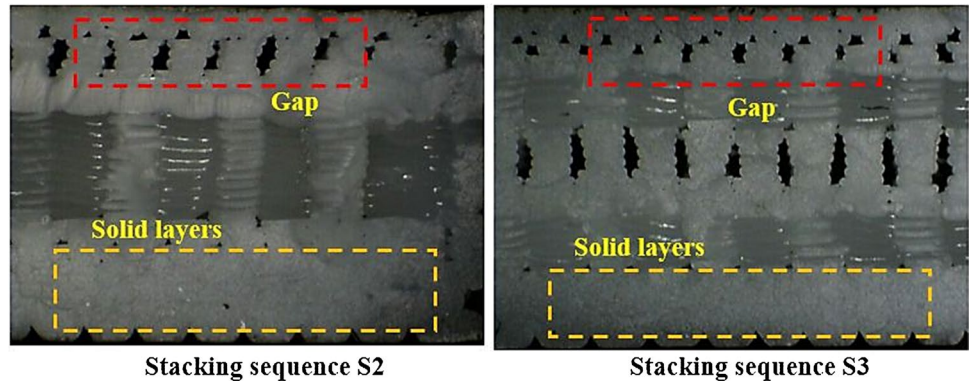**Fig. 16** Effect of infill density on tensile strength

Fig. 17 Cross-sectional view of samples having different infill density

For 0° raster orientation, the tensile load is applied along the direction of raster deposition. Due to the parallel alignment of raster deposition and loading direction, the individual raster is capable of bearing more load during tensile testing as well as the effect of raster bonding also minimized. For 45° raster orientation, the direction of the deposited raster is not parallel to the direction of the applied load. It is at an angle equal to the value of the raster angle considered i.e., applied load is not normal to the cross section of the raster can be seen in Fig. 20. In this case, the applied load is shared between raster and bonding between two rasters and due to weak bonding at the raster interface, shear failure occurs at the bonding region for parts with full infill. Raster orientation has no

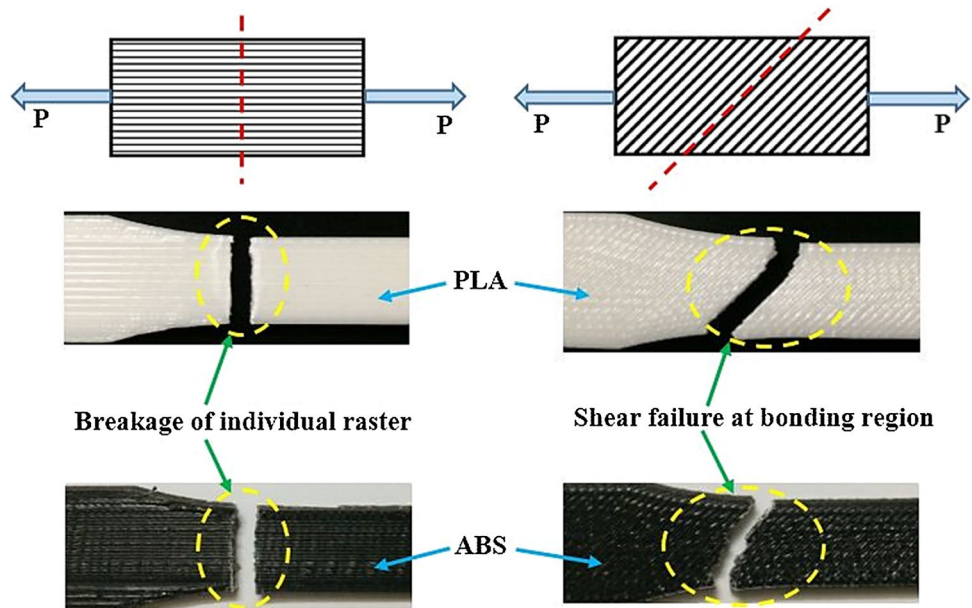**Fig. 18** Fractured surfaces for multi-infill pattern samples

Fig. 19 Effect of raster orientation on tensile strength

significant effect on tensile strength for multi-infill pattern parts at higher infill density i.e., at 90% infill density, stacking sequence S3 shows 35.1 MPa at 0° raster orientation and 36.4 MPa at 45° raster orientation; S4 shows 32 MPa at 0° raster orientation and 31.7 MPa at 45° raster orientation for PLA specimens. Whereas for ABS specimens, S4 shows 28.5 MPa at 0° raster orientation and 27.2 MPa at 45° raster orientation; S5 shows 27.6 MPa at 0° raster orientation and 27.1 MPa at 45° raster orientation. Figure 21 and Fig. 22 show fractured surfaces
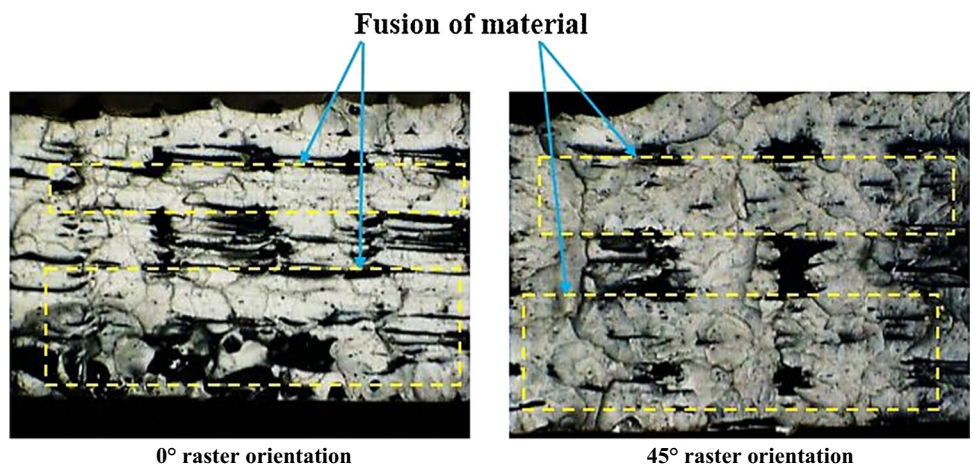
Fig. 20 Fracture pattern for different raster orientation

Fig. 21 Fractured surface of PLA sample having stacking sequence S3 at 90% infill density
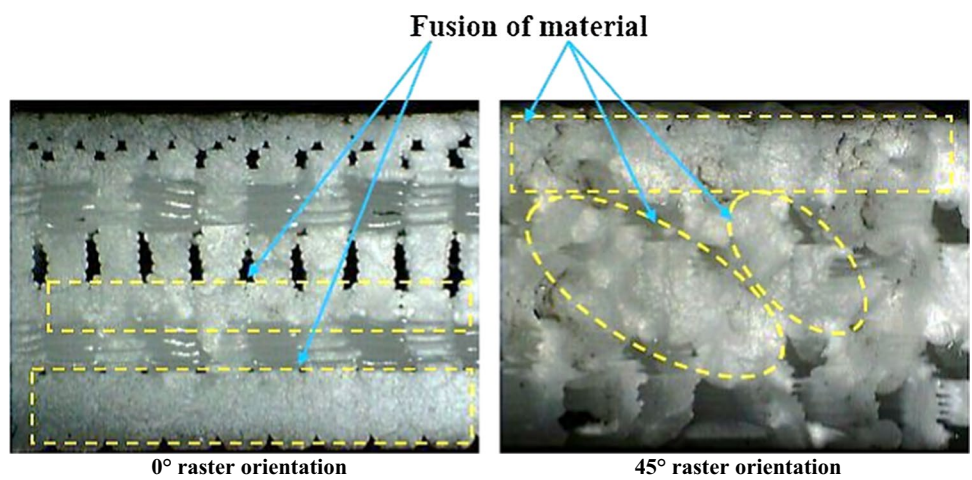
Fig. 22 Fractured surface of ABS sample having stacking sequence S5 at 90% infill density

of multi-infill pattern samples at 90% infill density. Fractographic analysis of fractured surfaces reveals that the load-bearing area remains almost the same for both raster orientations at 90% infill density. For 90% infill density, gap between rasters is very small and heat transfer from bed to layers causes fusion of material between two rasters in a layer, leads to lesser voids in the bottom region and some voids are observed in the top region. Hence, more material availability and inter raster material fusion at higher infill density offer almost the same load resisting area for both raster orientations, leads to similar tensile strength for multi-infill pattern samples.

4 Conclusion

The present study investigates the tensile behavior of FDM printed parts having multi-infill patterns and different stacking sequence of layer arrangement under different raster orientation and infill density. Based on the experimental results, the following major conclusions are drawn:

- At 0° raster orientation, parts having stacking sequence S1 offer the highest tensile strength, whereas part having stacking sequence S6 offers the lowest strength for all considered infill densities for both PLA and ABS specimens.
- Incorporation of grid layers decreases the tensile strength for parts having 0° raster orientation whereas, for 45° raster orientation, tensile strength is increased. The addition of grid layers in 45° raster orientation samples provides support to rectilinear layers and increases load resisting material, leads to an increase in tensile strength.
- Rectilinear layers undergo trans-raster failure, whereas grid layers exhibit failure due to breakage of bonding at raster meeting junction. Multi-infill pattern parts experienced mixed failure mechanism i.e., trans-raster as well as failure at raster meeting junction.
- No significant effect has been observed on strength due to raster orientation in multi-infill pattern parts at higher infill densities because of the very little gap between deposited rasters and almost the same load resisting area for both raster orientations.
- The highest strength offered by FDM printed samples for both the materials is less than that the strength of filament. For all considered print settings, PLA samples showed higher tensile strength than that of ABS samples.

Compliance with ethical standards

References

1. Akhoundi B, Behravesh AH, Bagheri Saed A (2018) Improving mechanical properties of continuous fiber-reinforced thermoplastic composites produced by FDM 3D printer. J Reinf Plast Compos 38(3):99–116. https://doi.org/10.1177/0731684418807300

2. Chua CK, Leong KF, Lim CS (2010) Rapid prototyping: principles and applications, 2nd edn. World Scientific, Singapore

3. Dave HK, Prajapati AR, Rajpurohit SR, Patadiya NH, Raval HK (2020) Investigation on tensile strength and failure modes of FDM printed part using in-house fabricated PLA filament. Adv Mater Process Technol. https://doi.org/10.1080/2374068X.2020.1829951

4. Popescu D, Zapciu A, Amza C, Baciu F, Marinescu R (2018) FDM process parameters influence over the mechanical properties of polymer specimens: a review. Polym Test 69:157–166. https://doi.org/10.1016/j.polymertesting.2018.05.020

5. Ahn SH, Montero M, Odell D, Roundy S, Wright PK (2002) Anisotropic material properties of fused deposition modeling ABS. Rapid Prototyp J 8:248–257. https://doi.org/10.1108/13552540210441166

6. Mohamed OA, Masood SH, Bhowmik JL (2016) Optimization of fused deposition modeling process parameters for dimensional accuracy using I-optimality criterion. Measurement 81:174–196. https://doi.org/10.1016/j.measurement.2015.12.011

7. Bamiduro O, Owolabi G, Haile MA, Riddick JC (2015) The influence of load direction, microstructure, raster orientation on the quasi-static response of fused deposition modeling ABS. Rapid Prototyp J 25:462–472. https://doi.org/10.1108/RPJ-04-2018-0087

8. Dawoud M, Taha I, Ebeid SJ (2016) Mechanical behaviour of ABS: An experimental study using FDM and injection moulding techniques. J Manuf Process 21:39–45. https://doi.org/10.1016/j.jmapro.2015.11.002

9. Uddin MS, Sidek MFR, Faizal MA, Ghomashchi R, Pramanik A (2017) Evaluating mechanical properties and failure mechanisms of fused deposition modeling acrylonitrile butadiene styrene parts. J Manuf Sci E 139:081018. https://doi.org/10.1115/1.4036713

10. Durgun I, Ertan R (2014) Experimental investigation of FDM process for improvement of mechanical properties and production cost. Rapid Prototyp J 20:228–235. https://doi.org/10.1108/RPJ-10-2012-0091

11. Li H, Wang T, Sun J, Yu Z (2018) The effect of process parameters in fused deposition modelling on bonding degree and mechanical properties. Rapid Prototyp J 24:80–92. https://doi.org/10.1108/RPJ-06-2016-0090

12. Casavola C, Cazzato A, Moramarco V, Pappalettere C (2016) Orthotropic mechanical properties of fused deposition modelling parts described by classical laminate theory. Mater Des 90:453–458. https://doi.org/10.1016/j.matdes.2015.11.009

13. Chacon JM, Caminero MA, Garcia-Plaza E, Nunez PJ (2017) Additive manufacturing of PLA structures using fused deposition modelling: effect of process parameters on mechanical properties and their optimal selection. Mater Des 124:143–157. https://doi.org/10.1016/j.matdes.2017.03.065

14. Rajpurohit SR, Dave HK (2018) Effect of process parameters on tensile strength of FDM printed PLA part. Rapid Prototyp J 24:1317–1324. https://doi.org/10.1108/RPJ-06-2017-0134

15. Dave HK, Patadiya NH, Prajapati AR, Rajpurohit SR (2019) Effect of infill pattern and infill density at varying part orientation on tensile properties of fused deposition modeling-printed poly-lactic acid part. P I Mech Eng C-J Mec. https://doi.org/10.1177/2F0954406219856383

16. Rodriguez JF, Thomas JP, Renaud JE (2001) Mechanical behavior of acrylonitrile butadiene styrene (ABS) fused deposition materials: Experimental investigation. Rapid Prototyp J 7:148–158. https://doi.org/10.1108/13552540110395547

17. Lederle F, Meyer F, Brunotte GP, Kaldun C, Hübner EG (2016) Improved mechanical properties of 3D-printed parts by fused deposition modeling processed under the exclusion of oxygen. Prog Addit Manuf 1:3–7. https://doi.org/10.1007/s40964-016-0010-y

18. Wu W, Geng P, Li G, Zhao D, Zhang H, Zhao J (2015) Influence of layer thickness and raster angle on the mechanical properties of 3D-printed PEEK and a comparative mechanical study between PEEK and ABS. Materials 8:5834–5846

19. Ziemian S, Okwara M, Ziemian CW (2015) Tensile and fatigue behavior of layered acrylonitrile butadiene styrene. Rapid Prototyp J 21:270–278. https://doi.org/10.1108/RPJ-09-2013-0086

20. Zaldivar RJ, Witkin DB, McLouth T, Patel DN, Schmitt K, Nokes JP (2017) Influence of processing and orientation print effects on the mechanical and thermal behavior of 3D-Printed ULTEM® 9085 Material. Addit Manuf 13:71–80. https://doi.org/10.1016/j.addma.2016.11.007

21. Alvarez C, Kenny L, Lagos C, Rodrigo F, Aizpun M (2016) Investigating the influence of infill percentage on the mechanical properties of fused deposition modelled ABS parts. Ing Invest 36:110–116

22. Shih CC, Burnette M, Staack D, Wang J, Tai BL (2019) Effects of cold plasma treatment on interlayer bonding strength in FFF process. Addit Manuf 25:104–111. https://doi.org/10.1016/j.addma.2018.11.005

23. Lee CY, Liu CY (2019) The influence of forced-air cooling on a 3D printed PLA part manufactured by fused filament fabrication. Addit Manuf 25:196–203. https://doi.org/10.1016/j.addma.2018.11.012

24. Bin Ishak I, Fleming D, Larochelle P (2019) Multiplane fused deposition modeling: a study of tensile strength. Mech Based Des Struct Mach 47:1–16. https://doi.org/10.1080/15397734.2019.1596127

25. Garg A, Bhattacharya A (2017) An insight to the failure of FDM parts under tensile loading: finite element analysis and experimental study. Int J Mech Sci 120:225–236. https://doi.org/10.1016/j.ijmecsci.2016.11.032

26. Taylor G, Wang X, Mason L, Leu MC, Chandrashekhara K, Schniepp T, Jones R (2018) Flexural behavior of additively manufactured Ultem 1010: experiment and simulation. Rapid Prototyp J 24:1003–1011. https://doi.org/10.1108/RPJ-02-2018-0037

27. Domingo-Espin M, Puigoriol-Forcada JM, Garcia-Granada AA, Llumà J, Borros S, Reyes G (2015) Mechanical property characterization and simulation of fused deposition modeling polycarbonate parts. Mater Des 83:670–677. https://doi.org/10.1016/j.matdes.2015.06.074

28. Bhandari S, Lopez-Anido R (2018) Finite element analysis of thermoplastic polymer extrusion 3D printed material for mechanical property prediction. Addit Manuf 22:187–196. https://doi.org/10.1016/j.addma.2018.05.009

29. Caminero MA, Chacón JM, García-Moreno I, Reverte JM (2018) Interlaminar bonding performance of 3D printed continuous fibre reinforced thermoplastic composites using fused deposition modelling. Polym Test 68:415–423. https://doi.org/10.1016/j.polymertesting.2018.04.038

30. Liao G, Li Z, Cheng Y, Xu D, Zhu D, Jiang S, Guo J, Chen X, Xu G, Zhu Y (2018) Properties of oriented carbon fiber/polyamide 12 composite parts fabricated by fused deposition modeling. Mater Des 139:283–292. https://doi.org/10.1016/j.matdes.2017.11.027

31. Zhang W, Cotton C, Sun J, Heider D, Gu B, Sun B, Chou TW (2018) Interfacial bonding strength of short carbon fiber/acrylonitrile-butadiene-styrene composites fabricated by fused deposition modeling. Compos B 137:51–59. https://doi.org/10.1016/j.compositesb.2017.11.018

32. Dickson AN, Barry JN, McDonnell KA, Dowling DP (2017) Fabrication of continuous carbon, glass and Kevlar fibre reinforced polymer composites using additive manufacturing. Addit Manuf 16:146–152. https://doi.org/10.1016/j.addma.2017.06.004

33. Li G, Zhao J, Jiang J, Jiang H, Wu W, Tang M (2018) Ultrasonic strengthening improves tensile mechanical performance of fused deposition modeling 3D printing. Int J Adv Manuf Tech 96:2747–2755. https://doi.org/10.1007/s00170-018-1789-0

34. Kerekes TW, Lim H, Joe WY, Yun GJ (2019) Characterization of process–deformation/damage property relationship of fused deposition modeling (FDM) 3D-printed specimens. Addit Manuf 25:532–544. https://doi.org/10.1016/j.addma.2018.11.008

35. Kozior T, Mamun A, Trabelsi M, Wortmann M, Lilia S, Ehrmann A (2019) Electrospinning on 3D printed polymers for mechanically stabilized filter composites. Polymers 11(12):2034. https://doi.org/10.3390/polym11122034

36. Kozior T, Blachowicz T, Ehrmann A (2020) Adhesion of three-dimensional printing on textile fabrics: inspiration from and for other research areas. J Eng Fibers Fabr 15:1558925020910875. https://doi.org/10.1177/1558925020910875

37. Kozior T, Mamun A, Trabelsi M, Sabantina L, Ehrmann A (2020) Quality of the surface texture and mechanical properties of FDM printed samples after thermal and chemical treatment. Stroj Vestnik J Mech Eng. https://doi.org/10.5545/sv-jme.2019.6322